AGU PUBLICATIONS

JGR

Journal of Geophysical Research: Space Physics

RESEARCH ARTICLE

10.1002/2016JA023091

Key Points:

- The effects of neutral winds and PPEFs on the nighttime ionosphere during 28–29 October 2003 were investigated
- The disturbances of the nighttime ionosphere in this event were mainly caused by TADs when the magnetic activity was weak
- Eastward PPEF with northward Bz contributed to the uplifting of the nighttime ionosphere at low latitudes on 29 October

Correspondence to:
J. Lei,
leijh@ustc.edu.cn

Citation:
Chen, X., J. Lei, W. Wang, A. G. Burns, X. Luan, and X. Dou (2016), A numerical study of nighttime ionospheric variations in the American sector during 28–29 October 2003, *J. Geophys. Res. Space Physics*, *121*, 8985–8994, doi:10.1002/2016JA023091.

Received 21 JUN 2016
Accepted 13 AUG 2016
Accepted article online 17 AUG 2016
Published online 16 SEP 2016

A numerical study of nighttime ionospheric variations in the American sector during 28–29 October 2003

Xuetao Chen[1], Jiuhou Lei[1,2,3], Wenbin Wang[4], Alan G. Burns[4], Xiaoli Luan[1], and Xiankang Dou[1]

[1]CAS Key Laboratory of Geospace Environment, School of Earth and Space Sciences, University of Science and Technology of China, Hefei, China, [2]Mengcheng National Geophysical Observatory, University of Science and Technology of China, Hefei, China, [3]Collaborative Innovation Center of Astronautical Science and Technology, Harbin, China, [4]High Altitude Observatory, National Center for Atmospheric Research, Boulder, Colorado, USA

Abstract Variations of nighttime F_2 peak height (h_mF_2) over the American sector during the 28–29 October 2003 storm period were investigated using the National Center for Atmospheric Research Thermosphere-Ionosphere Electrodynamics Global Circulation Model. The model was generally able to reproduce the ionospheric variations on 28–29 October 2003 observed by the ionosondes. A series of controlled model simulations were subsequently undertaken to examine the effects of electric fields and neutral winds on the ionosphere. The numerical experiments suggest that the dramatic nighttime increase of h_mF_2 on the storm day 29 October is mainly caused by traveling atmospheric disturbances (TADs) from the high latitudes of the Northern Hemisphere. However, the electric field plays an important role in causing the elevation of h_mF_2 in the equatorial region. The prompt penetration electric field (PPEF) associated with the southward component of the interplanetary magnetic field (B_z) is westward on the nightside, whereas when B_z reverses and becomes northward, the PPEF is westward in the premidnight and turns to eastward in the postmidnight. These PPEFs greatly affect the low-latitude ionosphere during storm time. On 28 October, even though the B_z disturbance was weak with a short duration of southward B_z, the TADs from the Southern Hemisphere can propagate to the Northern Hemisphere and result in the corresponding oscillations in the nightside h_mF_2.

1. Introduction

Two super geomagnetic storms on 29–31 October 2003 were produced by coronal mass ejections [*Gopalswamy et al.*, 2005]. The minimum of the *Dst* index reached below −400 nT during this period. The ionospheric response to these two superstorms has been comprehensively investigated over the years [*Abdu et al.*, 2007; *Balan et al.*, 2011; *Foster and Rideout*, 2005; *Lei et al.*, 2014, 2015; *Lin et al.*, 2005; *Tsurutani et al.*, 2008; *Zhao et al.*, 2005]. Prior to these two superstorms, a strong geomagnetic storm commenced at 6:10 UT on 29 October (storm 1; see Figure 1), in which the minimum *Dst* was −151 nT, associated with southward B_z of −40 nT. However, the ionospheric response to this strong storm has been rarely studied.

Lei et al. [2015] showed that the F_2 peak height (h_mF_2) was uplifted significantly during the main phase of the storm 1, while the peak density (N_mF_2) did not change much during the night. *Zhao et al.* [2005] proposed that the increase of nightside h_mF_2 at the magnetic equator probably resulted from an eastward prompt penetration electric field (PPEF) under the northward B_z condition. However, there is no theoretical result to test this hypothesis. *Lei et al.* [2015] showed that the nightside h_mF_2s were elevated to as much as 500 km at low and middle latitudes when B_z turned from southward to northward on 29 October 2003, whereas they still remained high when B_z turned southward. Thus, the rapid increase of nightside h_mF_2 might not only be controlled by PPEF but also influenced by other factors, such as, neutral winds. In addition, there were oscillations in h_mF_2 in the American sector on 28 October 2003 when geomagnetic activity was relatively weak and the southward interplanetary magnetic field (IMF) B_z was only a few nanotesla, i.e., the first shaded time interval in Figure 1. Due to insufficient observations, it is hard to isolate the effects of neutral winds and electric fields on the ionospheric response to the 28–29 October 2003 geomagnetic activity.

The aim of this paper is to address the following questions using the Thermosphere-Ionosphere Electrodynamics Global Circulation Model (TIEGCM) simulations: (1) Is the nighttime PPEF eastward when B_z is northward? (2) Is the uplifting of the nighttime ionosphere associated with an eastward PPEF during

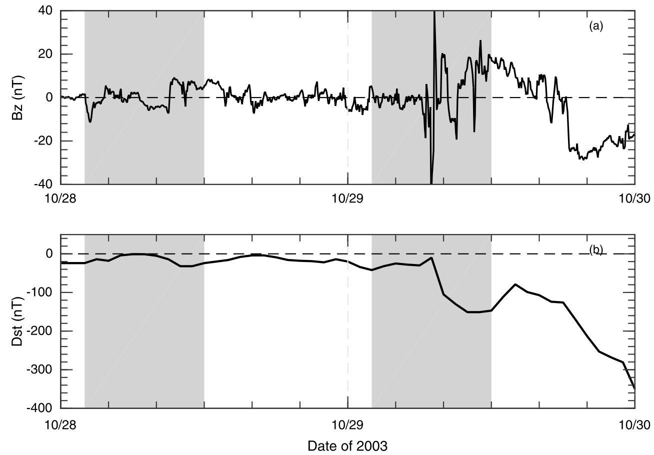

Figure 1. Variations of (a) the north-south component of the interplanetary magnetic field (IMF B_Z) observed by the ACE satellite and (b) *Dst* on 28 and 29 October 2003. The two shaded intervals are the periods in which we are interested.

the northward B_z period? (3) What is the main factor in causing the nighttime ionospheric disturbance when geomagnetic activity is weak?

2. TIEGCM Numerical Experiments

The National Center for Atmospheric Research TIEGCM [*Richmond et al.*, 1992; *Roble et al.*, 1988] is a comprehensive, first-principles, three-dimensional, nonlinear representation of the coupled thermosphere and ionosphere system that includes a self-consistent solution of the middle- and low-latitude dynamo fields. The model uses a semi-implicit, fourth-order, centered finite difference scheme to solve the three-dimensional momentum, energy, and continuity equations for neutral and ion species. In this paper, we used a grid with vertical resolution of one fourth scale height with a total of 57 pressure levels and horizontal resolution of 2.5° × 2.5° in geographic coordinates. The magnetospheric convection inputs at high latitudes are provided by the Weimer model [*Weimer*, 2005], and migrating diurnal and semidiurnal tides are imposed at the lower boundary using the global scale wave model [*Hagan et al.*, 1999].

To investigate the relative importance of neutral winds and electric fields on the ionospheric variations, we carried out three numerical experiments: (1) a simulation with both $E \times B$ drift and meridional winds (Run 1), (2) a simulation with meridional winds but without $E \times B$ drift (Run 2), and (3) a simulation with $E \times B$ drift but without meridional winds (Run 3) in the *F* region ion continuity equation.

3. Results and Discussions

Figure 2 shows a comparison of h_mF_2 and N_mF_2 between the ionosonde data and the TIEGCM simulations (Run 1, blue lines; Run 2, green lines) at Dyess, Eglin, and Jicamarca on 28 and 29 October. The geographic and geomagnetic coordinates of these four ionosonde stations are listed in Table 1. The predicted results (gray lines) from the International Reference Ionosphere (IRI) model [*Bilitza et al.*, 2014] during quiet time are also shown in Figure 2 to represent the reference, due to the absence of ionosonde observations during the quiet time condition in October 2003. The ionosonde data obtain from Global Ionospheric Radio Observatory of the University of Mass Lowell [*Reinisch and Galkin*, 2011] and the manually scaled ionograms are used to analyze the behaviors of N_mF_2 and h_mF_2. In this study, we focus on the ionospheric variations during 2:00–12:00 when these stations are at local night. The observed h_mF_2s on 29 October showed significant increases following a transient decrease during 8:00–10:00 UT at four stations. However, at Jicamarca, h_mF_2 oscillated many times when h_mF_2 was uplifted to 400 km. On 28 October, the wave-like oscillations of nighttime h_mF_2 during 4:00–12:00 UT were seen at Dyess and Ramey (there were no observations at Eglin and Jicamarca during this period). Obviously, these observed disturbances in nighttime h_mF_2s on 28 and 29 October were not found in the quiet time IRI results. It is expected since these h_mF_2 disturbances could be associated with geomagnetic activity. Hereafter we will not further discuss the IRI results. We first compare the TIEGCM simulated h_mF_2 with the observed values during 6:00–12:00 UT on 29 October. In the Run 1, the h_mF_2s showed clear increases at 8:00 UT at all stations. However, at Dyess and Eglin, the h_mF_2 showed a sharp decrease to 200 km at 9:00 UT after the profound increase, which is different from the observations. Besides the remarkable increase of h_mF_2 at the onset of the storm 1 at all stations, the oscillations seen in the ionosonde nighttime h_mF_2 on 28 October were captured by the model in Run 1.

The TIEGCM also captured the main features observed in N_mF_2. For instance, the simulated N_mF_2s (blue lines) showed similar diurnal variation to the observed ones. However, there were still considerable differences between simulations and observations, especially during 12:00–20:00 UT on 29 October when lower N_mF_2

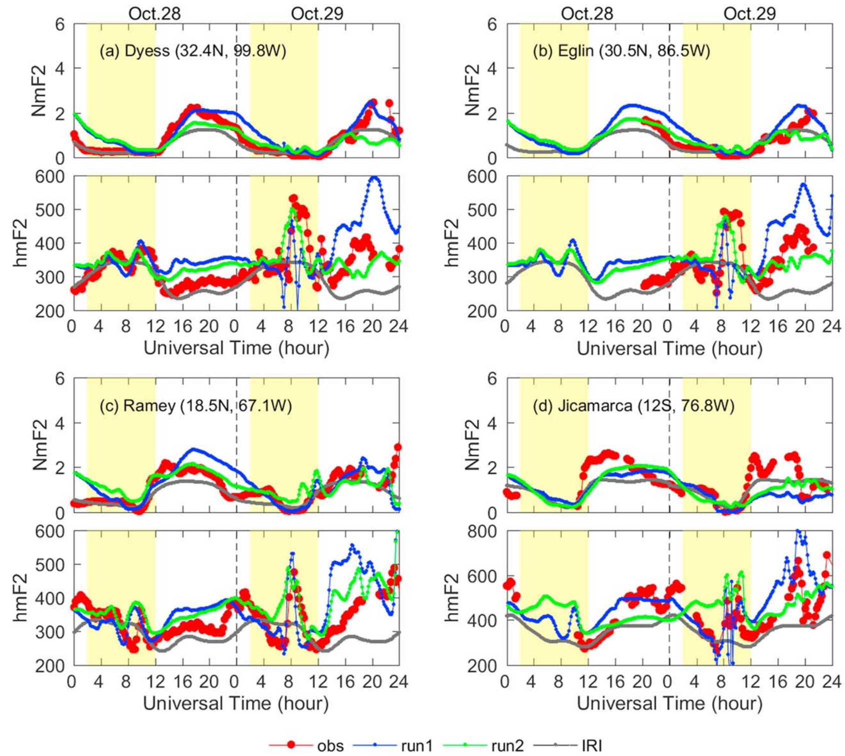

Figure 2. Comparison of observations and simulations of peak density N_mF_2 (in units of 10^{12} m^{-3}) and peak height h_mF_2 (in units of km) at Dyess, Eglin, Ramey, and Jicamarca on 28 and 29 October 2003. Red lines represent observations obtained from ionosonde measurements; gray lines represent the predictions from the International Reference Ionosphere model during quite time; blue lines represent the simulated results of Run 1, and green lines represent the simulation results with no $E \times B$ drift (Run 2) in the ion continuity equation. The intervals on which we focused are marked by the yellow bars.

and higher h_mF_2 from the simulation than observations were seen at Jicamarca. Except for some deviations between simulations and observations, the model reproduces the main features observed in h_mF_2 and N_mF_2 at all stations on 28 and 29 October. Note that both the observed and simulated nighttime N_mF_2s did not show the dramatic changes that h_mF_2 did. In this storm h_mF_2 was more sensitive to dynamic effects than N_mF_2 was during this nighttime period. Because of this disparity in the response of N_mF_2 and h_mF_2 to dynamic forcing, we will concentrate on the variations of h_mF_2 to explore the ionospheric dynamic processes in the remainder of the paper.

We used the TIEGCM to study the mechanisms that cause the ionospheric disturbances on 28 and 29 October. H_mF_2s from Run 2 are shown in Figure 2 (green line). On 28 October, the nighttime h_mF_2 from Run 2 showed the wave-like oscillations, which were similar to those from Run 1 at low- and middle-latitude stations, except that the increased magnitude of h_mF_2 from Run 2 was a little smaller than that from Run 1. On 29 October the maximum of the h_mF_2 during 7:00–10:00 UT at each station from Run 2 was similar to that from Run 1, except at Ramey. Although the maximum h_mF_2 from Run 2 was lower than that from Run 1 at Ramey, the increase of h_mF_2 caused by neutral wind was obvious. Thus, the sharp h_mF_2 increases during 7:00–10:00 UT were associated with neutral winds, since electric field was turned off in Run 2.

Table 1. Geographic and Geomagnetic Coordinates of Dyess, Eglin, Ramey, and Jicamarca

Station	Geographic Latitude	Geographic Longitude	Magnetic Latitude	Magnetic Longitude
Dyess	32.4°N	99.8°W	41.4°N	32.0°W
Eglin	30.5°N	86.5°W	40.4°N	16.8°W
Ramey	18.5°N	67.1°W	28.8°N	5.0°E
Jicamarca	12.0°S	76.8°W	1.7°S	5.0°W

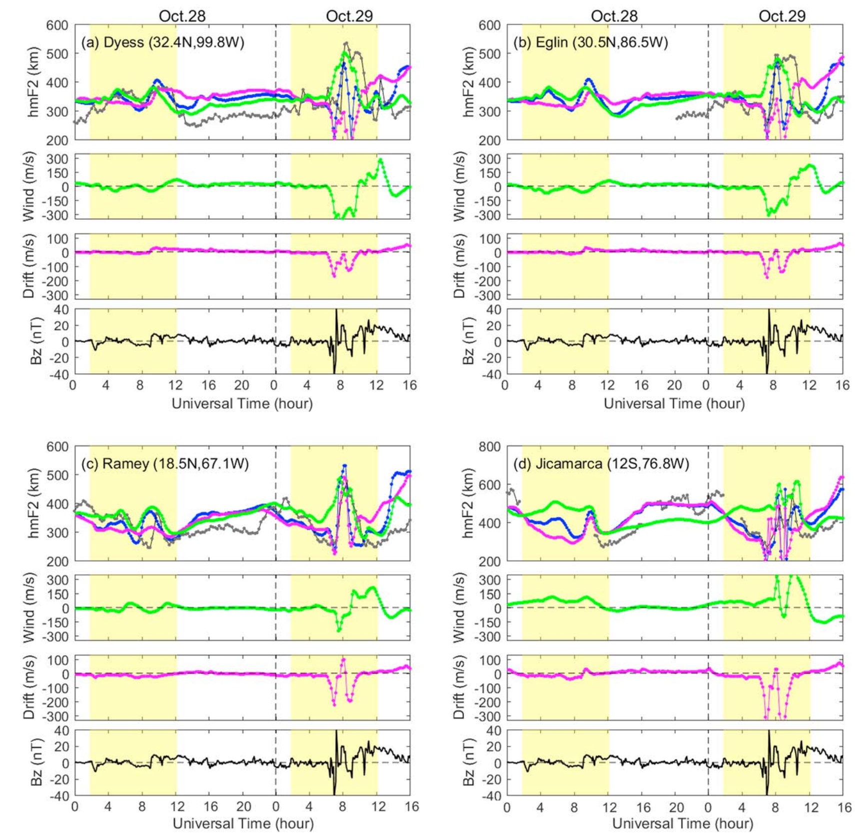

Figure 3. Comparison of the observed h_mF_2 (gray lines) and simulated h_mF_2s from three TIEGCM simulations: Run 1 (blue), Run 2 (green), and Run 3 (magenta) on 28 and 29 October 2003. Vertical $E \times B$ drifts (upward positive) and meridional winds (northward positive) at 400 km from Run 1 are shown in the second and third panels in each subplot, respectively. The B_z variations are shown in bottom panel in each subplot.

Figure 3 further shows the comparison of observed h_mF_2s and simulated h_mF_2s from three simulations at four stations. The vertical $E \times B$ drifts and meridional winds calculated from Run 1 are also shown in this figure to illustrate their contribution to h_mF_2 variations. Unlike the results of Run 1 and Run 2, the wave-like oscillations were absent in h_mF_2 in Run 3 (with $E \times B$ drift and without meridional winds) on 28 October. Thus, our simulations indicate that the wave-like oscillations in nighttime h_mF_2 on 28 October were mainly associated with the neutral winds. However, the variations of the electric field can further modulate the wind-induced h_mF_2 disturbance, especially at lower latitudes (Ramey and Jicamarca). On 29 October, as mentioned above, the simulated h_mF_2s from Run 1 and Run 2 were generally consistent with the observations. In Figure 3, it is clear that the sharp increase in h_mF_2 during 7:00–10:00 UT was attributed to the strong equatorward surge of winds with speeds larger than 200 m/s.

In Figures 2–3, there are substantial differences in the simulated h_mF_2s between Run 2 and Run 1, particularly at around 7:00 and 9:00 UT on 29 October. The obvious decline of the h_mF_2 is only seen in Run 1, which suggests that the downward $E \times B$ drifts were the dominant cause for the decline at these UTs. This is immediately evident from the results in Run 3, in which $E \times B$ drifts were included but meridional winds were turned off. As shown in the bottom panels in each subplot of Figure 3, $E \times B$ drifts were downward when B_z was southward. The downward $E \times B$ drift was caused by the dawn-dusk PPEF or westward electric field on the nightside [*Fejer et al.*, 1979; *Scherliess and Fejer*, 1997]. In addition to the prevalent downward $E \times B$ drift on the nightside, the $E \times B$ drifts turned upward at Ramey and Jicamarca at 8:00 UT when B_z was northward. These upward $E \times B$ drifts contribute to the uplifting of ionosphere. Referring back to Figure 2, the simulated h_mF_2s at ~9:00 UT from Run 1 were too low as compared with the observations at each station except at Ramey. Although at ~7:00 UT the simulated h_mF_2s were also lower than that in observations at Dyess and Eglin, they showed similar pattern as observed by the ionosondes. At these UTs, the downward $E \times B$ drifts from Run1 were probably strong. These discrepancies indicate that the PPEF might be overestimated in the TIEGCM.

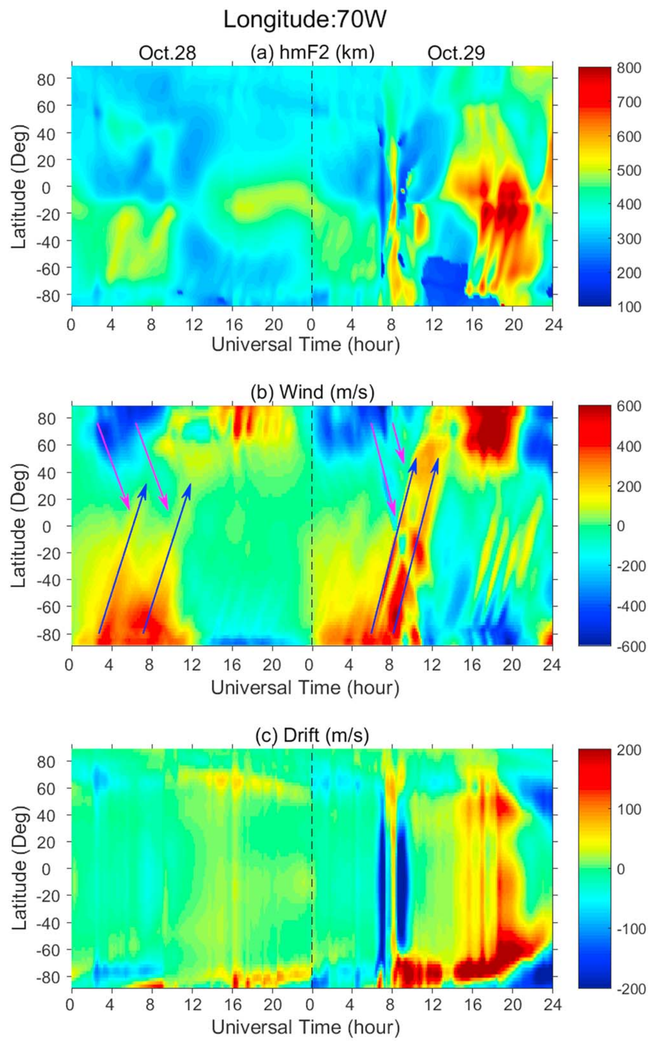

Figure 4. The modeled h_mF_2, meridional winds (northward positive), and $E \times B$ drifts (upward positive) as functions of geographic latitude and universal time along the longitude of 70°W on 28 and 29 October 2003. The TADs investigated in this study are marked by arrows.

The effects of neutral winds and electric fields on the ionosphere have been studied previously [*Balan et al.*, 2013; *Lei et al.*, 2008]. The equatorward wind can raise the ionosphere along the magnetic field line to high altitudes and reduce chemical loss rate [*Balan et al.*, 2010]. An upward $E \times B$ drift due to eastward electric field tends to increase h_mF_2, whereas a westward electric field has the opposite effect. However, the N_mF_2 did not show such obvious change as seen in h_mF_2s at night when the electron density profile was flat [*Lei et al.*, 2008]. In our investigation, the effects of neutral winds and electric fields have significant latitudinal variations. As mentioned above, the neutral winds caused significant uplifting of the ionosphere at Dyess and Eglin on 29 October and also introduced oscillations in the nighttime ionosphere at Dyess and Ramey on 28 October. On 29 October, at Ramey, the combined effect of equatorward winds and upward $E \times B$ drifts caused a strong increase in h_mF_2. Neutral winds became ineffective at Jicamarca due to the fact that geomagnetic field line at the magnetic equator is horizontal, whereas the electric field can modulate the h_mF_2 effectively. Thus, in this event, the disturbances of the nighttime ionosphere were mainly caused by neutral winds in the middle and low latitudes, while the electric field further modulates the nighttime ionosphere.

Latitudinal variations of meridional winds, electric fields, and h_mF_2 from Run 1 at the longitude of 70°W are shown in Figure 4. When B_z is southward or interplanetary shock encounter the Earth, Joule heating at high latitudes would increase suddenly due to the magnetosphere interacting with IMF or the enhanced solar wind. The enhanced Joule heating can expand the upper atmosphere and produce traveling atmospheric disturbances (TADs) [*Fuller-Rowell et al.*, 1994]. These large-scale waves (horizontal wavelength over 1000 km) can propagate far away from the source due to weak dissipation [*Mayr et al.*, 1990]. The TADs originating in the polar regions can transfer momentum and energy to lower latitudes [*Richmond*, 1978] and drive equatorward (poleward) winds which uplift (suppress) the ionosphere along the magnetic field line in the middle and low latitudes. On 28 October, when B_z turned southward, the TADs originated in both hemispheres. Two TADs (magenta arrows) that were generated in the North Pole drove equatorward winds, resulting in elevations of the ionosphere in the Northern Hemisphere. Correspondingly, two TADs (blue arrows) originating from the Southern Hemisphere resulted in neutral wind disturbances in the Northern Hemisphere, which is consistent with the investigation of *Fuller-Rowell et al.* [1994], who showed that TADs can penetrate to the opposite hemisphere and change the winds to the poleward direction for a few hours.

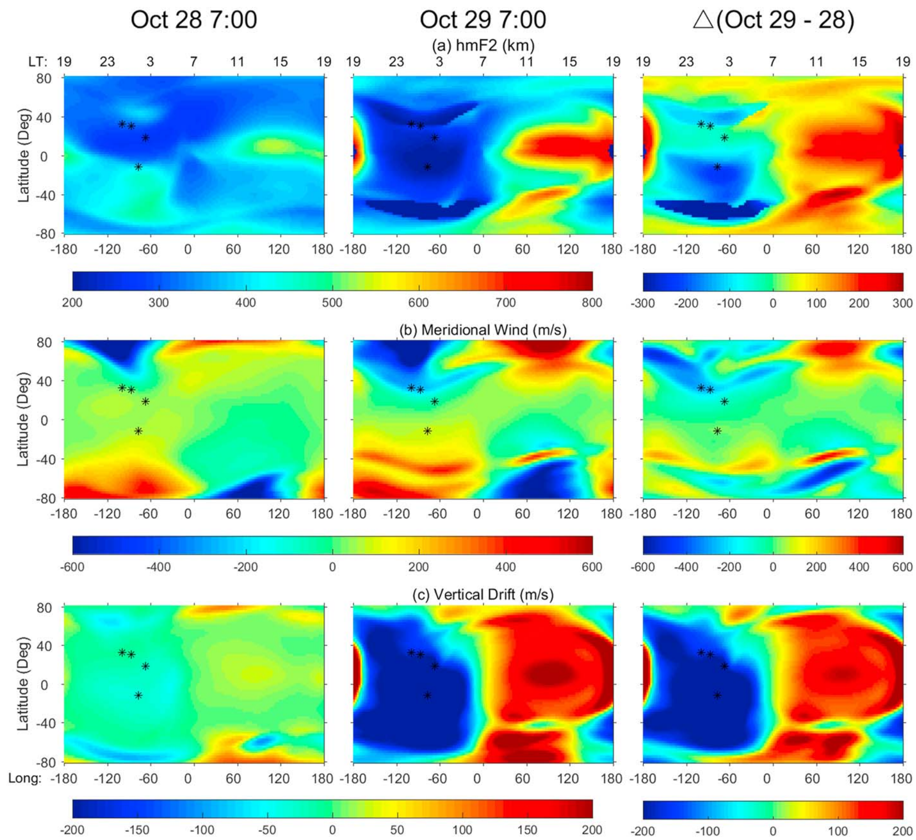

Figure 5. Global maps of modeled (a) h_mF_2, (b) meridional winds (northward positive), and (c) $E \times B$ drifts (upward positive) at 7 UT on 28 and 29 October. The differences at 7 UT between 28 and 29 October are in the right panel. Black dots stand for ionosonde stations.

The wave-like oscillations of h_mF_2 in the Northern Hemisphere during around 4:00–10:00 UT were caused by the two transequator TADs, since the vertical $E \times B$ drift was weak at low and middle latitudes. At 7:00 UT on 29 October, when B_z turned southward and reached -40 nT, the TADs were also observed. The multiple TADs generated in the South Pole even propagated into the high latitudes of the Northern Hemisphere and drove strong poleward winds that resulted in rapid decreases in h_mF_2s in the Northern Hemisphere during 10:00–13:00 UT. These variations of ionosphere were consistent with the observations in ionosondes. Thus, these wind surges play important role in producing oscillations in the nighttime ionosphere in the Northern Hemisphere on 28 and 29 October. The vertical $E \times B$ drift shows complicated patterns associated with the changes of B_z. During 6:00–10:00 UT on 29 October, strong vertical $E \times B$ drift caused by PPEF expanded to middle latitudes from the equator during a dramatic disturbance of B_z. Thus, the PPEF impacted the ionosphere over a wide range of latitudes. The effects of electric field and neutral winds on the ionosphere had obvious latitudinal variations. The vertical $E \times B$ drift became strong around the equator during 6:00–10:00 UT on 29 October. However, the maximum of ionosphere disturbance caused by neutral wind was in the middle latitudes on 28 October. These simulated results were consistent with the mechanisms that vertical $E \times B$ drift is proportional to cos$I$ and the vertical ion drag caused by neutral wind is proportional to sin2I, where I is the dip angle. Thus, during storm time the ionosphere was profound impacted by the PPEF at the equator. At higher latitudes, the PPEFs also can moderate h_mF_2, while the neutral winds play a major role in this region. When the geomagnetic activity was weak, the TADs also generated in both polar regions with southward B_z and dominated the ionosphere in the middle and low latitudes.

To gain more information about global wind fields and electric fields, we chose two UTs: 7:00 UT on 29 October when southward B_z reached its minimum and 8:00 UT on 29 October when B_z turned northward after a few hours of southward B_z.

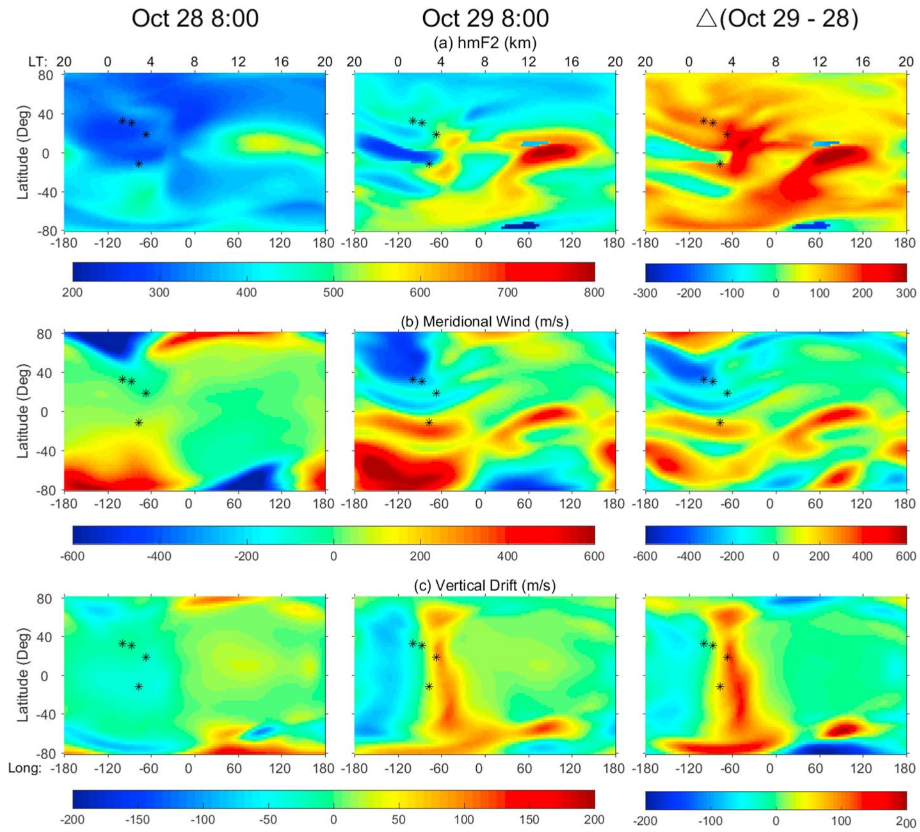

Figure 6. Global maps of modeled (a) h_mF_2, (b) meridional winds (northward positive), and (c) $E \times B$ drifts (upward positive) at 8 UT on 28 and 29 October. The differences at 8 UT between 28 and 29 October are in the right panel. Black dots stand for ionosonde stations.

Figure 5 shows the global maps of h_mF_2, meridional winds, and vertical $E \times B$ drifts obtained from Run 1 at 7:00 UT on 28 and 29 October. We first look at the simulated results on 28 October. The evident summer-to-winter background winds are seen in the left panel of Figure 5b. The nighttime transequatorial wind from the summer hemisphere to the winter hemisphere caused the asymmetry in nighttime h_mF_2 (left panel of Figure 5a). At 7:00 UT on 29 October, when B_z was southward, Joule heating generated noticeable TADs in the polar region. The TADs are remarkable at night, whereas the dayside TADs are probably restricted by poleward background winds and enhanced ion drag. The vertical $E \times B$ drift was greatly enhanced with respect to its value on 28 October. The $E \times B$ drift was downward in the night (20:00–6:00 LT) and upward in the daytime (7:00–19:00 LT). This was caused by the profound dawn-dusk PPEF during southward B_z. The most intense upward $E \times B$ drift was in the postdusk sector, which is consistent with previous observations [*Abdu et al.*, 2008]. The right panel of Figure 5a shows the difference of h_mF_2 at 7:00 UT between 28 and 29 October, which was negative on the nightside and positive on the dayside. These features of h_mF_2 are consistent with the observations [*Zhao et al.*, 2005], which showed significant decreases of h_mF_2 at Jicamarca (nightside) and increases of h_mF_2 over East Asian stations (dayside) associated with the large changes in vertical $E \times B$ drifts. The greatest uplifting of the ionosphere was caused by the prereversal enhancement of the upward $E \times B$ drift in the postsunset hours. Thus, the ionosphere was dominated by the PPEFs in the middle and low latitudes before the TADs propagate to these latitudes from the polar regions.

The global maps of h_mF_2, meridional winds, and vertical $E \times B$ drifts obtained from Run 1 at 8:00 UT on 28 and 29 October are shown in Figure 6. Clearly, the nightside TADs in both Southern and Northern Hemispheres propagated toward the equator. The changes of neutral winds in the two hemispheres were different. The nighttime TAD in the Northern Hemisphere was weaker than that in the Southern Hemisphere. The strong dayside TADs in the Southern Hemisphere also propagated to the equator, even though the background wind was poleward on the dayside. However, the daytime TAD generated from the North Pole cannot even drive to the equator.

Fuller-Rowell et al. [1996] proposed that the neutral winds in the two hemispheres are different due to the seasonal differences of polar energy injection and background winds. The hemispheric asymmetry of the energy injection on 29–31 October 2003 has been demonstrated by *Zhao et al*. [2005] using the ion temperature measurements made by the Defense Meteorological Satellite Program, which showed that the energy injection in the Southern Hemisphere was more significant than that in the Northern Hemisphere. The hemispheric difference in the TADs is mainly attributed to the asymmetric energy injection in the polar regions. Referring back to Figure 4, the transequator TAD turned the winds to poleward in the Northern Hemisphere, while the effect of transequator TAD in the Southern Hemisphere was too weak to cause ionospheric changes when the ionosphere was in the nighttime sector. This suggests that the TADs primarily drive equatorward winds in both hemispheres and subsequent poleward winds in the winter hemisphere at night.

Previous studies show that both the thermosphere and ionosphere have extensive responses to TADs on 28–29 October 2003 [e.g., *Ding et al*., 2007; *Guo et al*., 2014; *Qian et al*., 2012]. The characteristic behavior of h_mF_2 in relation to B_z has been investigated by *Blanch and Altadill* [2012] for the middle latitudes. They proposed that the uplifting of the ionosphere may be caused by equatorward TADs in middle latitudes when $B_z \leq -10$ nT. In our study, the simulated results demonstrate that equatorward TAD can cause significant increase of h_mF_2 in middle and low latitudes in both hemispheres. After the ionosphere uplifts, the transequator TAD resulted in rapid decrease of h_mF_2 in the Northern Hemisphere. Thus, when B_z turned to southward, the ionosphere in the summer hemisphere was uplifted due to the equatorward TADs; in addition to increase of h_mF_2 for a few hours in the winter hemisphere, the subsequent transequator TADs from the opposite hemisphere could cause rapid decline of h_mF_2.

The global maps of vertical $E \times B$ drifts calculated from Run 1 at 7:00 UT and 8:00 UT on 29 October are shown in Figures 5c and 6c, respectively. The difference of the vertical $E \times B$ drifts between 7:00 UT and 8:00 UT on 29 October is obvious. The $E \times B$ drift change was downward before midnight and upward after midnight, which indicates that PPEF was reversed in the premidnight. In addition to the different morphology of $E \times B$ drifts, the magnitude of $E \times B$ drifts during northward B_z was distinctly smaller than that during southward B_z. Previous studies have shown that the polarity of PPEF reverses when B_z turns northward [*Kelley et al*., 1979].

To address the effects of electric fields and neutral winds on the nighttime ionosphere with northward B_z, we will concentrate on the differences between 28 and 29 October at 8:00 UT that are shown in the right panel in each subplot of Figure 6. Neutral winds had a strong equatorward enhancement at night in the middle and low latitudes. The upward enhancement of vertical $E \times B$ drift appeared after midnight, while the downward $E \times B$ drift intensified slightly before midnight. The whole ionosphere showed significant uplifting, except for a small region where the equatorward wind enhancement was absent. The greatest increase of nightside h_mF_2 was seen in low latitudes at around 5:00 LT. It was driven by the combined effect of upward $E \times B$ drift and equatorward wind. The PPEF has an immediate response to the variation of B_z [*Kikuchi et al*., 1996]. However, the TADs over the low latitudes are typically delayed for a few hours from the energy injection in polar regions [*Fuller-Rowell et al*., 2002]. As discussed above, the equatorward wind was followed by a poleward wind that was driven by transequator TAD in the winter hemisphere. The oscillating B_z would cause a complicate variation of the ionosphere.

Figure 7 shows the high-latitude potential maps obtained from Run 1 at 7:00 and 8:00 UT on 28 and 29 October in the Northern Hemisphere. On 28 October, when the geomagnetic activity was weak, the two-cell structure of the potential was obvious in the polar region. The main feature of any two-cell structure is that the maximum and minimum potentials are located at the dawn and dusk sides, respectively. The association between the potential and electric fields can be presented by the equation $E = -\nabla\phi$ where E is the electric field and ϕ is the potential. According to the potential structure, there is a dawn-dusk electric field in the polar region. On 29 October, when B_z was southward (7:00 UT), the two-cell structure developed and extended to lower latitudes. These potential maps indicate that the dawn-dusk electric fields penetrated to low latitudes with southward B_z during the storm [*Kikuchi et al*., 1996]. When B_z turned northward (8:00 UT), the two-cell structure was destroyed. The negative peak of potential was still at high latitudes, while the positive peak of potential shifted to middle latitudes due to the influence of B_y. Although the potential was even weaker than it had been in the low geomagnetic activity before the storm, the electric field was still able to penetrate to low latitudes. The PPEF was westward before midnight and eastward after midnight in the equatorial region. This electric field contributed to the profound nighttime h_mF_2 variations in the low latitudes.

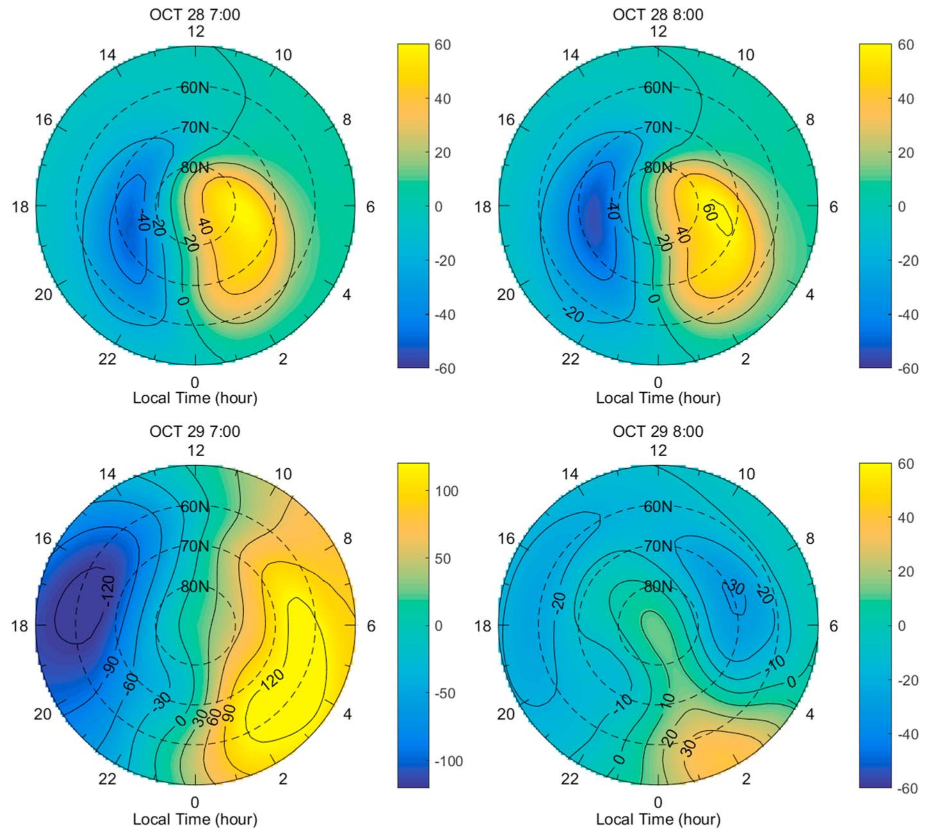

Figure 7. Global maps of electric potential (in units of KV) in middle and high latitudes at 7 UT and 8 UT on 28 and 29 October.

4. Summary

In this paper, the TIEGCM simulations were used to investigate the nighttime ionospheric variations seen in the ionosonde data over the American sector during a major geomagnetic storm event on 28 and 29 October 2003. The main conclusions of this study are listed as follows:

1. The TIEGCM can generally reproduce the nighttime observations from ionosonde measurements in the American sector on 28 and 29 October. The difference between the simulation and observation may be associated with an overestimation of the PPEF during the southward B_z period on 29 October.
2. The controlled experiments using the TIEGCM demonstrated that the dramatic increases of h_mF_2 observed by ionosondes were mainly caused by TADs which were triggered by the polar Joule heating associated with southward B_z during the storm, whereas the electric field played a primary role in the h_mF_2 elevation at equatorial and low latitudes.
3. On 28 October, even though southward B_z was weak and had a short duration, the TADs from the Southern Hemisphere propagated to the Northern Hemisphere and subsequently caused the oscillations in the nightside h_mF_2.
4. When B_z reversed from southward to northward directions, the PPEF kept westward in the premidnight sector but became eastward in the postmidnight sector (around 2–6 LT). The resultant PPEF during the northward B_z condition affected the nighttime variations of the ionosphere at low latitudes.

Acknowledgments
The model data are available upon request. We acknowledge Global Ionospheric Radio Observatory (GIRO) and GIRO Principal Investigator B.W. Reinisch of the University of Massachusetts Lowell (http://ulcar.uml.edu/DIDBase/ and http://spase.info/VWO/NumericalData/GIRO/CHARS.PT15M) for making the ionosonde data available and B. Zhao for his kind help in processing the ionosonde data. This work was supported by the National Natural Science Foundation of China (41325017, 41274157, 41274158, and 41421063), the Project of Chinese Academy of Sciences (KZZD-EW-01), the National Key Basic Research Program of China (2012CB825605), the Fundamental Research Funds for the Central Universities, and the Thousand Young Talents Program of China. The National Center for Atmospheric Research is sponsored by the National Science Foundation.

References

Abdu, M. A., T. Maruyama, I. S. Batista, S. Saito, and M. Nakamura (2007), Ionospheric responses to the October 2003 superstorm: Longitude/local time effects over equatorial low and middle latitudes, *J. Geophys. Res.*, *112*, A10306, doi:10.1029/2006JA012228.
Abdu, M. A., et al. (2008), Abnormal evening vertical plasma drift and effects on ESF and EIA over Brazil-South Atlantic sector during the 30 October 2003 superstorm, *J. Geophys. Res.*, *113*, A07313, doi:10.1029/2007JA012844.

Balan, N., K. Shiokawa, Y. Otsuka, T. Kikuchi, D. Vijaya Lekshmi, S. Kawamura, M. Yamamoto, and G. J. Bailey (2010), A physical mechanism of positive ionospheric storms at low latitudes and midlatitudes, *J. Geophys. Res.*, *115*, A02304, doi:10.1029/2009JA014515.

Balan, N., M. Yamamoto, J. Y. Liu, Y. Otsuka, H. Liu, and H. Lühr (2011), New aspects of thermospheric and ionospheric storms revealed by CHAMP, *J. Geophys. Res.*, *116*, A07305, doi:10.1029/2010JA016399.

Balan, N., Y. Otsuka, M. Nishioka, J. Y. Liu, and G. J. Bailey (2013), Physical mechanisms of the ionospheric storms at equatorial and higher latitudes during the recovery phase of geomagnetic storms, *J. Geophys. Res. Space Physics*, *118*, 2660–2669, doi:10.1002/jgra.50275.

Bilitza, D., D. Altadill, Y. Zhang, C. Mertens, V. Truhlik, P. Richards, L.-A. McKinnell, and B. Reinisch (2014), The International Reference Ionosphere 2012—A model of international collaboration⋆, *J. Space Weather Space Clim.*, *4*, 12, doi:10.1051/swsc/2014004.

Blanch, E., and D. Altadill (2012), Midlatitude *F* region peak height changes in response to interplanetary magnetic field conditions and modeling results, *J. Geophys. Res.*, *117*, A12311, doi:10.1029/2012JA018009.

Ding, F., W. Wan, B. Ning, and M. Wang (2007), Large-scale traveling ionospheric disturbances observed by GPS total electron content during the magnetic storm of 29–30 October 2003, *J. Geophys. Res.*, *112*, A06309, doi:10.1029/2006JA012013.

Fejer, B. G., C. A. Gonzales, D. T. Farley, M. C. Kelley, and R. F. Woodman (1979), Equatorial electric fields during magnetically disturbed conditions: 1. The effect of the interplanetary magnetic field, *J. Geophys. Res.*, *84*(A10), 5797–5802, doi:10.1029/JA084iA10p05797.

Foster, J. C., and W. Rideout (2005), Midlatitude TEC enhancements during the October 2003 superstorm, *Geophys. Res. Lett.*, *32*, L12S04, doi:10.1029/2004GL021719.

Fuller-Rowell, T. J., M. V. Codrescu, R. J. Moffett, and S. Quegan (1994), Response of the thermosphere and ionosphere to geomagnetic storms, *J. Geophys. Res.*, *99*(A3), 3893–3914, doi:10.1029/93JA02015.

Fuller-Rowell, T. J., M. V. Codrescu, H. Rishbeth, R. J. Moffett, and S. Quegan (1996), On the seasonal response of the thermosphere and ionosphere to geomagnetic storms, *J. Geophys. Res.*, *101*(A2), 2343–2353, doi:10.1029/95JA01614.

Fuller-Rowell, T. J., G. H. Millward, A. D. Richmond, and M. V. Codrescu (2002), Storm-time changes in the upper atmosphere at low latitudes, *J. Atmos. Sol. Terr. Phys.*, *64*(12–14), 1383–1391, doi:10.1016/S1364-6826(02)00101-3.

Gopalswamy, N., S. Yashiro, Y. Liu, G. Michalek, A. Vourlidas, M. L. Kaiser, and R. A. Howard (2005), Coronal mass ejections and other extreme characteristics of the 2003 October–November solar eruptions, *J. Geophys. Res.*, *110*, A09S15, doi:10.1029/2004JA010958.

Guo, J., H. Liu, X. Feng, W. Wan, Y. Deng, and C. Liu (2014), Constructive interference of large-scale gravity waves excited by interplanetary shock on 29 October 2003: CHAMP observation, *J. Geophys. Res. Space Physics*, *119*, 6846–6851, doi:10.1002/2014JA020255.

Hagan, M. E., M. D. Burrage, J. M. Forbes, J. Hackney, W. J. Randel, and X. Zhang (1999), GSWM-98: Results for migrating solar tides, *J. Geophys. Res.*, *104*(A4), 6813–6827, doi:10.1029/1998JA900125.

Kelley, M. C., B. G. Fejer, and C. A. Gonzales (1979), An explanation for anomalous equatorial ionospheric electric fields associated with a northward turning of the interplanetary magnetic field, *Geophys. Res. Lett.*, *6*(4), 301–304, doi:10.1029/GL006i004p00301.

Kikuchi, T., H. Lühr, T. Kitamura, O. Saka, and K. Schlegel (1996), Direct penetration of the polar electric field to the equator during a DP 2 event as detected by the auroral and equatorial magnetometer chains and the EISCAT radar, *J. Geophys. Res.*, *101*(A8), 17,161–17,173, doi:10.1029/96JA01299.

Lei, J., W. Wang, A. G. Burns, S. C. Solomon, A. D. Richmond, M. Wiltberger, L. P. Goncharenko, A. Coster, and B. W. Reinisch (2008), Observations and simulations of the ionospheric and thermospheric response to the December 2006 geomagnetic storm: Initial phase, *J. Geophys. Res.*, *113*, A01314, doi:10.1029/2007JA012807.

Lei, J., W. Wang, A. G. Burns, X. Yue, X. Dou, X. Luan, S. C. Solomon, and Y. C. M. Liu (2014), New aspects of the ionospheric response to the October 2003 superstorms from multiple-satellite observations, *J. Geophys. Res. Space Physics*, *119*, 2298–2317, doi:10.1002/2013JA019575.

Lei, J., Q. Zhu, W. Wang, A. G. Burns, B. Zhao, X. Luan, J. Zhong, and X. Dou (2015), Response of the topside and bottomside ionosphere at low and middle latitudes to the October 2003 superstorms, *J. Geophys. Res. Space Physics*, *120*, 6974–6986, doi:10.1002/2015JA021310.

Lin, C. H., A. D. Richmond, R. A. Heelis, G. J. Bailey, G. Lu, J. Y. Liu, H. C. Yeh, and S. Y. Su (2005), Theoretical study of the low- and midlatitude ionospheric electron density enhancement during the October 2003 superstorm: Relative importance of the neutral wind and the electric field, *J. Geophys. Res.*, *110*, A12312, doi:10.1029/2005JA011304.

Mayr, H. G., I. Harris, F. A. Herrero, N. W. Spencer, F. Varosi, and W. D. Pesnell (1990), Thermospheric gravity waves: Observations and interpretation using the transfer function model (TFM), *Space Sci. Rev.*, *54*(3), 297–375, doi:10.1007/bf00177800.

Qian, L., A. G. Burns, H. Liu, and P. C. Chamberlin (2012), Effect of a solar flare on a traveling atmospheric disturbance, *J. Geophys. Res.*, *117*, A10319, doi:10.1029/2012JA017806.

Reinisch, B. W., and I. A. Galkin (2011), Global Ionospheric Radio Observatory (GIRO), *Earth Planets Space*, *63*(4), 377–381, doi:10.5047/eps.2011.03.001.

Richmond, A. D. (1978), Gravity wave generation, propagation, and dissipation in the thermosphere, *J. Geophys. Res.*, *83*(A9), 4131–4145, doi:10.1029/JA083iA09p04131.

Richmond, A. D., E. C. Ridley, and R. G. Roble (1992), A thermosphere/ionosphere general circulation model with coupled electrodynamics, *Geophys. Res. Lett.*, *19*(6), 601–604, doi:10.1029/92GL00401.

Roble, R. G., E. C. Ridley, A. D. Richmond, and R. E. Dickinson (1988), A coupled thermosphere/ionosphere general circulation model, *Geophys. Res. Lett.*, *15*(12), 1325–1328, doi:10.1029/GL015i012p01325.

Scherliess, L., and B. G. Fejer (1997), Storm time dependence of equatorial disturbance dynamo zonal electric fields, *J. Geophys. Res.*, *102*(A11), 24,037–24,046, doi:10.1029/97JA02165.

Tsurutani, B. T., et al. (2008), Prompt penetration electric fields (PPEFs) and their ionospheric effects during the great magnetic storm of 30–31 October 2003, *J. Geophys. Res.*, *113*, A05311, doi:10.1029/2007JA012879.

Weimer, D. R. (2005), Improved ionospheric electrodynamic models and application to calculating Joule heating rates, *J. Geophys. Res.*, *110*, A05306, doi:10.1029/2004JA010884.

Zhao, B., W. Wan, and L. Liu (2005), Responses of equatorial anomaly to the October–November 2003 superstorms, *Ann. Geophys.*, *23*(3), 693–706, doi:10.5194/angeo-23-693-2005.